Electromechanical Modes Identification Based on an Iterative Eigenvalue Decomposition of the Hankel Matrix

Alejandro Zamora-Mendez, *Member, IEEE*, Rodrigo D. Reyes de Luna, *Student Member, IEEE*, José Antonio de la O Serna, *Senior Member, IEEE*, Joe H. Chow, *Life Fellow, IEEE*, and Mario R. Arrieta Paternina, *Member, IEEE*

***Abstract*—This paper proposes a novel strategy to precisely extract modal patterns from non-stationary multi-component signals associated with electromechanical oscillations in large-scale power systems. The strategy is composed of two stages: (*i*) a time-frequency representation (TFR) method; and (*ii*) an energy-based operator. The former is equipped with a multivariate and iterative eigenvalue decomposition of the Hankel matrix (IEVDHM) that captures the swing dynamics as a mono-component signal criterion is fulfilled, meanwhile the latter instantaneously estimates the modal information (damping and frequency) through the discrete energy separation algorithm (DESA) that implements the discrete-time energy operators derived from the Teager-Kaiser energy operators (TKEO). The attained results and their comparisons with state-of-the-art techniques confirm the effectiveness and performance of the proposed strategy to demodulate synthetic, simulated and real oscillating signals, even under high noisy conditions, and to be a useful tool for off-line contingency analysis thanks to the capability of differentiating concurrent modes with close frequencies.**

***Index Terms*—Electromechanical oscillations, eigenvalue decomposition, Hankel matrix, non-stationary signals, time-frequency representation.**

I. Introduction

THE extraction of modal parameters in power systems after a large disturbance provides a paramount information for the situational awareness and decision-making process in monitoring and control centers; since poor damped modes, or even worse, negatively damped modes may lead to the system separation or complete black out. This may also damage, in an irreversible way, the generator's rotors whose cost is very high [1]. To ensure the correct monitoring of power systems around the world, wide-area monitoring systems (WAMS) have been implemented with the purpose of collecting electric parameters such as frequency, voltages, currents, angles, powers through phasor measurement units (PMUs) installed in different electric substations [2]–[4]. Thus the more PMUs installed, the better observability of the system.

The main feature of PMUs is that all measurements have their own time stamp, allowing an analysis or comparison with other PMU measurements [5]. Currently, most of WAMS are implementing different digital signal processing techniques derived from the information registered by the PMU, aiming to extract modal information of the measured signals and determinate the power system dynamic performance. So far, there are many algorithms and mathematical methods to capture the necessary information for monitoring the system. The goal of this paper is focused on proposing an algorithm to analyze the signals captured by PMUs in order to extract their modal information, which is a valuable tool to improve situational awareness of system operators to make correct control decisions.

The extraction of modal information in power systems has been mainly focused by two approaches: model-based and measurement-based methods. The former is focused on a linearized model of the electric power system around an operating point, and the latter fits the measurements onto linear or non-linear models [6], [7]. Such measurements are evaluated by linear ringdown analysis methods (oscillatory response after disturbance), which use strategies of digital signal processing for identifying modal information (amplitude, frequency, damping and phase).

Considering the increasing digitalization in power systems, it is necessary to develop and implement the most accurate, efficient, reliable and robust mathematical algorithms for the adequate monitoring of its performance. Reaching these demands, poses great challenges today due to the large number of options available and limitations in hardware and software.

Manuscript received 27 May 2021; revised 31 October 2021 and 7 February 2022; accepted 19 March 2022. Date of publication 23 March 2022; date of current version 22 December 2022. This work was supported by the Project Support Program for Research and Technological Innovation of UNAM (DGAPA, PAPIIT-2021) under Project TA101421. Paper no. TPWRS-00833-2021. *(Corresponding author: Mario Roberto Arrieta Paternina.)*

Alejandro Zamora-Mendez is with the Electrical Engineering Faculty, Michoacan University of Saint Nicholas of Hidalgo (UMSNH), Morelia, Michoacan 58030, Mexico (e-mail: azamoram@umich.mx).

Rodrigo D. Reyes de Luna and José Antonio de la O Serna are with the Electrical Engineering, Autonomous University of Nuevo Leon, Monterrey, NL 66450, Mexico (e-mail: rodrigo.reyesd@uanl.edu.mx; jdelao@ieee.org).

Joe H. Chow is with the Department of Electrical, Computer and Systems Engineering, Rensselaer Polytechnic Institute (RPI), Troy, NY 12180-3590 USA (e-mail: chowj@rpi.edu).

Mario R. Arrieta Paternina is with the Department of Electrical Engineering, National Autonomous University of Mexico, Mexico City 04510, Mexico (e-mail: mra.paternina@fi-b.unam.mx).

Color versions of one or more figures in this article are available at https://doi.org/10.1109/TPWRS.2022.3161598.

Digital Object Identifier 10.1109/TPWRS.2022.3161598

A. State-of-the-Art

Most of the measured signals from dynamic systems as large electric power systems are non-stationary, therefore they contain time-varying parameters [8]. Consequently, the time–frequency representation (TFR) emerges as a reliable tool that fulfills such requirements showing frequency components and their features at different time instants. It is useful to analyze non-stationary signals in time and frequency domains making possible the extraction of modal information [9].

The basic technique for time-frequency analysis of non-stationary signals is a spectrogram, which is derived from short-time Fourier transform (STFT) [10]. In the STFT method, a signal can be considered as stationary within an analysis window. The spectrum analysis based on Fourier transformation is applied to short-time windowed signals whose length of analysis buffer in time is directly related to the frequency resolution. This analysis provides poor resolution in the frequency-domain but high time-resolution. Moreover, there is no standard rule for determining the length and type of window function in the STFT for the analysis of non-stationary signals. Therefore, the STFT is not suitable for efficient analysis of non-stationary signals. To overcome this resolution issue, the adaptive short-time Fourier transform (ASTFT) has been proposed [11]. However, it was observed that these techniques hinged on STFT are computationally expensive [12]. The afore-mentioned limitations are overcome for non-stationary signal analysis by the wavelet transform (WT) [13], [14]. Wavelet basis functions can be considered adaptive window functions providing an alternative way of signal analysis that can be performed for a given point in time using many scales [15]. This multi-resolution property of the WT solves the issue of fixed resolution in time and frequency domains when fixed analysis windows are used [16], [17].

A different type of TFR is the Wigner-Ville distribution (WVD) method [10], [18]. Theoretically, the WVD method exhibits particularly good resolutions in both time and frequency. It is highly suitable for mono-component linear frequency modulated signals. But, for nonlinear frequency modulated signals and multi-component non-stationary signals, the WVD method generates cross-terms which can be considered as a serious disadvantage of this method [12], [19], [20].

Another time-frequency technique for non-stationary and non-linear signal analysis is the Hilbert-Huang transform (HHT) which decomposes a multi-component non-stationary signal using the empirical mode decomposition (EMD) technique [21], [22]. The mono-component signals drawn by the EMD technique are known as intrinsic mode functions (IMFs). The Hilbert transform (HT) is applied to these IMFs to compute their amplitude envelope and instantaneous frequency. Both the amplitude envelope and the instantaneous frequency of IMFs are then employed to gain the HHT-based TFR. However, the IMFs obtained by using the EMD method suffer from the mode mixing issue, resulting in improper TFR [23]. Nevertheless, different efforts as the proposal in [24] seek to overcome this issue by enhancing the EMD method, this is known as ensemble empirical mode decomposition (EEMD) and is proposed to deal with noisy signal analysis, reducing the mode mixing issue [25].

In [26], a new adaptive method named variational mode decomposition (VMD) is proposed aiming to determine the relevant frequency bands adaptively by estimating the corresponding modes concurrently and balancing errors among them. This is achieved by reconstructing a given input signal $x(t)$ using constrained optimization techniques. Afterwards, [27] introduces the identification of electromechanical oscillatory modes in power systems. Its applicability is demonstrated in a real WAMS and the instantaneous modal information is derived via HT.

Alternatively, the instantaneous modal information of a signal can also be extracted by the Teager-Kaiser algorithm [28]. Being one of the most important characteristics, the ability to precisely track the instantaneous frequency of the signal in those cases where there are single sinusoidal components that are constant or rapidly changing in frequency. Since the introduction of the Teager-Kaiser energy operator (TKEO) together with its continuous and discrete-time energy operators that allow providing instantaneous frequency and amplitude estimates via the continuous and discrete energy separation algorithms (CESA and DESA, respectively) [29], [30], numerous applications have been reported, such as in power systems [31], where the detection issue of instabilities is addressed in a fast way. Such applications in the power system community have been limited to detect low-frequency oscillations and to estimate the oscillating frequency. Nevertheless, the authors have not found any prior proposals in the literature for damping estimation via the energy operators.

Besides the methods described previously, three well-known linear methods stand out to perform a ringdown analysis, these are the Prony's method (PM), eigensystem realization algorithm (ERA), and matrix pencil (MP), whose straightforward implementations are summarized in [6]. They are also employed to identify electromechanical modes after a large disturbance takes place in the system.

B. Contribution

In modern power grids, phenomena such as the sparsity of the electrical networks with long transmission lines, weak interconnections or highly loaded corridors limiting the power transfer, may lead to trigger the undesirable presence of lightly damped electromechanical oscillations, making their study a critical aspect for planning and operation [6]. Thus, these phenomena contribute to decrease the oscillatory stability of modern power systems, causing major transients due to the presence of nonlinear and non-stationary components which can not be analyzed by traditional linear analysis methods [6]. In this context, this paper takes advantages of the recent advances in nonlinear and non-stationary time-frequency analyses to study and characterize complex oscillatory phenomena.

The novelty of this investigation lies in proposing a new TFR for non-stationary multi-signal analysis which performs a multivariate form of the iterative eigenvalue decomposition of the Hankel matrix (IEVDHM) method, instead of univariate as in [9]; also the multivariate IEVDHM is followed by a multivariate DESA implementation that facilitates the extraction

of instantaneous modal parameters, instead of the Hilbert estimation. Thus, our contribution introduces the multivariate IEVDHM-DESA method in the power system literature.

Besides its successful and recent implementation of the univariate IEVDHM technique in different fields (biomedical engineering, speech signals and time-series forecasting) [32]–[35], its capability to provide mechanisms to analyze and characterize nonlinear oscillating signals and non-stationary processes motivates us to bring it into the power system community as a powerful tool to properly and precisely achieve TFRs, specifically in the identification of modes with electromechanical nature.

Furthermore, thanks to a multi-channel Hankel form followed by the extraction of significant information conveyed by the SVD and its orthogonality property, our proposal achieves a multi-variate approach and enables deriving a reduced-order Hankel matrix to next gain all mono-component signals, and in turn, these mono-components are processed using the discrete-time energy operators and the DESA to instantaneously obtain modal parameters (frequency and damping). Thus, this research also exploits the advantages of the energy operators beyond the detection of low-frequency oscillations and the estimation of the oscillating frequency [31]. This is done by incorporating high order energy operators to the signal model, interpreting their physical meaning (the second, third and fourth order energy operators are referred as position, velocity, and acceleration), and relating the energy operators to the changes in frequency and damping (not only frequency and amplitude) [30], [36], [37].

The potential and effectiveness of the proposed strategy (IEVDHM-DESA) are unveiled and tested under simulated and real data environments, where high noisy conditions and a recorded real event of an actual WAMS are considered. Finally, our proposal exposes accurate approximations in extracting modal information, as well as low computational burden in comparison with the well-known Prony method.

C. Structure of the Paper

The remaining sections of the paper are structured as follows. Section II presents a complete description of the IEVDHM method to process single and multiple channels. Section III describes the fundamentals of the energy separation algorithm based on the Teager-Kaiser energy operator for continuous and discrete time. Section IV exhibits the performance of the IEVDHM-DESA-based strategy for time-frequency analyses in synthetic, simulated, and real signals. Finally, the concluding remarks are summarized in Section V.

II. Iterative Eigenvalue Decomposition of Hankel Matrix

In this section, an iterative approach to decompose a set of multi-component non-stationary signals into mono-component signals is proposed to extract the oscillatory characteristics of each mono-component such as frequency and damping. The proposed is an iterative approach based on repeatedly performing eigenvalue decomposition (EVD) of the Hankel matrix (HM), initially constructed from the samples of a set of multi-component signals.

A. Extraction of Components From a Multi-Component Signal

Since Prony's method was developed [38], the power system measured response's signals can generally be described as the sum of K primitive signals with amplitude and frequency modulations as

$$s(n) = \sum_{k=1}^{K} A_k e^{\sigma_k n} cos(2\pi f_k n + \phi_k) \tag{1}$$

where A_k, f_k, σ_k, and ϕ_k are the amplitude, frequency, damping, and phase of the k-th signal component, respectively.

For the extraction of components from a multi-component signal described as in (1), the square Hankel matrix $\mathbf{H}$ of size $N \times N$ and consisting of $2N-1$ elements can be constructed from the signal $s(n)$ which is spanning N samples as in [9]. This is represented as follows:

$$\mathbf{H} = \begin{bmatrix} s(0) & s(1) & \cdots & s(N-1) \\ s(1) & s(2) & \cdots & s(N) \\ \vdots & \vdots & \ddots & \vdots \\ s(N-1) & s(N) & \cdots & s(2N-2) \end{bmatrix} \tag{2}$$

where $n = 0, 1, \ldots, M-1, M \geq 2N-1$ and N is an even number. Thus, the square Hankel matrix constructed from a real signal will be a symmetric matrix, i.e. $\mathbf{H} = \mathbf{H}^T$, where T denotes the transpose operator. The EVD of the square matrix $\mathbf{H}$ can be expressed as [9]

$$\mathbf{H} = \mathbf{V}\mathbf{\Lambda}\mathbf{V}^T \tag{3}$$

where $\mathbf{\Lambda}$ is a diagonal matrix with N real eigenvalues λ_i, $i = 1, 2, \ldots, N$. $\mathbf{V}$ is an orthogonal matrix that consists of real eigenvectors such that $\mathbf{v}_i \cdot \mathbf{v}_j = 0$.

The EVD of the square matrix $\mathbf{H}$ results in $2K$ nonzero eigenvalues (≥ 0) and the corresponding eigenvectors are orthogonal for $j \neq k$. Accordingly, the $2K$ eigenvalues and their corresponding eigenvectors are respectively expressed as

$$\lambda_{s,(2k+r-2)} = \lambda_{s_k,r} \tag{4}$$

$$\mathbf{v}_{s,(2k+r-2)} = \mathbf{v}_{s_k,r} \tag{5}$$

for $r = 1, 2$.

Thus, the k-th mono-component signal of $s(n)$ can be extracted by creating a modified eigenvalue diagonal matrix $\tilde{\mathbf{\Lambda}}_{s_k}$ that preserves only the k-th non-zero eigenvalue pair of $\mathbf{\Lambda}$ as follows:

$$\tilde{\mathbf{\Lambda}}_{s_k} = diag(0, \ldots, 0, \lambda_{s,2k-1}, \lambda_{s,2k}, 0, \ldots, 0) \tag{6}$$

where $diag(\cdot)$ denotes the diagonal matrix and the Hankel matrix $\tilde{\mathbf{H}}_{s_k}$ is defined by [32]

$$\begin{aligned} \tilde{\mathbf{H}}_{s_k} &= \mathbf{V}\tilde{\mathbf{\Lambda}}_{s_k}\mathbf{V}^T \\ &= \lambda_{s,k}\mathbf{v}_k\mathbf{v}_k^T + \lambda_{s,N-k+1}\mathbf{v}_{N-k+1}\mathbf{v}_{N-k+1}^T \end{aligned} \tag{7}$$

where $N \geq F_s/\Delta F_{s,min}$, with F_s and $\Delta F_{s,min}$ standing for the sampling frequency and the minimum frequency separation between the components of $s(n)$. Then, the k-th mono-component signal of $s(n)$ is extracted by taking the mean of elements of

skew diagonals of $\tilde{\mathbf{H}}_{s_k}$ as follows [32]:

$$\hat{s}_k(n) = mean\left(\sum_j \sum_i \tilde{\mathbf{H}}_{s_k}(i,j)\right) \tag{8}$$

with the constraint that $i+j = n+2$ and $i,j = 1,\ldots,N$.

Thus, each extracted component $\hat{s}_k(n), \forall k$ is checked for the *mono-component signal criteria* (*MSC*) defined as follows [9]:

1) The magnitude of the difference between the number of zero crossings N_{zc} and the number of local extrema N_{le} (local minima and local maxima) of the extracted component denoted by $D_n = |N_{zc} - N_{le}|$, which can be equal to zero or one.
2) The number of significant eigenvalues pairs λ_s obtained by performing the EVD to the Hankel matrix and denoted by $D_r = \lambda_s$ is equal to one.

If an extracted component of $s(n)$ does not satisfy the MSC, the process of constructing the Hankel matrix performing EVD and component extraction using (3), (6) and (7), referred as *'Iteration'*, is repeated by treating the extracted component as a multi-component signal for the next *Iteration*. The *iterations* are repeated until all extracted components of $s(n)$ comply with the MSC. Thanks to the iterative performed by the IEVDHM method and the selection of the largest eigenvalue is defined as criterion, spurious modes do not appear.

B. Extraction of Components From Multiple Signals

The multivariate representation of the IEVDHM method considers multiple output channels shaped in the following matrix form:

$$\mathbf{S}_m = [\mathbf{s}^{\{1\}}\ \mathbf{s}^{\{2\}}\ \cdots\ \mathbf{s}^{\{q\}}\ \cdots\ \mathbf{s}^{\{m\}}] \tag{9}$$

where $\mathbf{S}_m \in \Re^{N\times m}$ is shaped by m column arrays corresponding to single channels, and the q-th column is denoted by a single signal as $\mathbf{s}^{\{q\}} = [s(0)\ s(1)\ \cdots\ s(N-1)]^T$.

Once each output channel corresponding to PMU signals is assembled into $\mathbf{S}_m$, a block Hankel matrix $\tilde{\mathbf{H}}_m \in \Re^{mN\times N}$ is built using submatrices Hankel $\mathbf{H}_m \in \Re^{N\times N}$ for each single channel, as follows:

$$\tilde{\mathbf{H}}_m = [\mathbf{H}_1 \quad \mathbf{H}_2 \quad \cdots \quad \mathbf{H}_m]^T \tag{10}$$

Then, (10) can also be expressed in terms of the samples contained in $\mathbf{S}_m$, as:

$$\tilde{\mathbf{H}}_m = \begin{bmatrix} s_m(0) & s_m(1) & \cdots & s_m(N-1) \\ s_m(1) & s_m(2) & \cdots & s_m(N) \\ \vdots & \vdots & \ddots & \vdots \\ s_m(N-1) & s_m(N) & \cdots & s_m(2N-2) \end{bmatrix}^T \tag{11}$$

To extract the significant information of the assembled Hankel matrix, a singular value decomposition (SVD) is applied to $\tilde{\mathbf{H}}_m$ which is given by

$$\tilde{\mathbf{H}}_m \approx \tilde{\mathbf{U}}\tilde{\mathbf{\Sigma}}\tilde{\mathbf{V}}^T \tag{12}$$

where $\tilde{\mathbf{U}} \in \Re^{N\times mN}$, and $\tilde{\mathbf{\Sigma}} \in \Re^{mN\times N}$, and $\tilde{\mathbf{V}} \in \Re^{N\times N}$ contains in its diagonal N real eigenvalues σ_i, $i = 1,2,\ldots,N$. The application of SVD over the block Hankel matrix ($\tilde{\mathbf{H}}_m$) for multiple signals allows our proposal to extract the significant information from multiple signals assembled into the data matrix ($\mathbf{S}_m$), this is due to the orthogonality property of SVD. Thus, we adopt a hybrid multivariate analysis using SVD and EVD, since it enables deriving a reduced-order Hankel matrix ($\tilde{\mathbf{H}}^{red}_{m,k}$) to next evaluate the *MSC criteria* for all mono-component signals, and also it allows to simplify the analysis performed by EVD to only the signals with the higher energy. Then, the first k-th singular values are selected by using their magnitudes as criterion, resulting in a reduced-order Hankel matrix such that

$$\tilde{\mathbf{H}}^{red}_{m,k} = \tilde{\mathbf{V}}\tilde{\mathbf{\Sigma}}^{red}_{m,k}\tilde{\mathbf{V}}^T \tag{13}$$

By taking advantage of the orthogonality in matrix $\tilde{\mathbf{V}}$, a set of k matrices Hankel is derived per singular value from (13), resulting in:

$$\tilde{\mathbf{H}}^{red}_{m,k} = \sigma_{m,1}\mathbf{v}_1\mathbf{v}_1^T + \sigma_{m,2}\mathbf{v}_2\mathbf{v}_2^T + \cdots + \sigma_{m,k}\mathbf{v}_k\mathbf{v}_k^T \tag{14}$$

Afterwards a modal decomposition can be applied to the k-th square matrix $\sigma_{m,k}\mathbf{v}_k\mathbf{v}_k^T$, in a similar way than in (7), and the iterative process in (8) can be conveyed preventing the presence of spurious contributions. Thus, the reduced matrix contains the samples of the k-th mono-components that closely represent the underlying electromechanical dynamics of the system in an optimal set of mono-component estimates. Next iterations are similar to the multi-component signal in Section II-A.

III. Fundamentals of the Energy Separation Algorithm Based on the Teager-Kaiser Energy Operator

Once the oscillating modes are correctly estimated by the multi-dimensional IEVDHM, the instantaneous modal features' extraction for the k-th mode represented by $s_k(t)$ may be estimated via the Teager-Kaiser energy operator (TKEO). This nonlinear energy operator for continuous-time and discrete-time signals was developed by Teager [39] and subsequently introduced systematically by Kaiser [28]. The TKEO is highly effective for numerous applications including the development of the energy separation algorithm (ESA) for demodulating AM-FM signals, tracking speech modulations, and detecting events in non-stationary signals.

A. Continuous-Time Energy Separation

In continuous-time, the TKEO is applied to the estimation of amplitude and frequency using the CESA. Thus, the continuous-time energy operator must be defined for the k-th mono-component signal in (1) (with $t = n/F_s$) such that [30]

$$\Psi[\hat{s}_k(t)] = [\dot{\hat{s}}_k(t)]^2 - \hat{s}_k(t)\ddot{\hat{s}}_k(t) \tag{15}$$

where $\dot{\hat{s}}_k(t)$ and $\ddot{\hat{s}}_k(t)$ are the first and second derivatives of $\hat{s}_k(t)$, respectively. Then, applying Ψ to $\hat{s}_k$ and $\dot{\hat{s}}_k$, yields [30]

$$\begin{aligned} \Psi[\hat{s}_k(t)] &= A_k^2\omega_k^2 e^{2\sigma t} \\ \Psi[\dot{\hat{s}}_k(t)] &= A_k^2\omega_k^4 e^{2\sigma t}\left(1 + \frac{\sigma_k^2}{\omega_k^2}\right) \end{aligned} \tag{16}$$

Now, assuming that the mode is lightly damped, i.e. $(\sigma_k/\omega_k)^2 << 1$, the instantaneous frequency (ω_k) and amplitude (A_k) can be estimated by the CESA as [30]:

$$\omega_k(t) \approx \sqrt{\frac{\Psi[\dot{\hat{s}}_k(t)]}{\Psi[\hat{s}_k(t)]}} = \omega_k\sqrt{1+\frac{\sigma_k^2}{\omega_k^2}}$$
$$|A_k(t)|e^{\sigma_k t} \approx \frac{\Psi[\hat{s}_k(t)]}{\sqrt{\Psi[\dot{\hat{s}}_k(t)]}} = \frac{|A_k(t)|e^{\sigma_k t}}{\sqrt{1+\frac{\sigma_k^2}{\omega_k^2}}} \quad (17)$$

Thus, the damping estimate may be computed as

$$\hat{\sigma}_k(t) = -\frac{1}{2}\frac{d\log\Psi[s_k(t)]}{dt} \quad (18)$$

and the frequency estimate as

$$\hat{f}_k(t) = \frac{\omega_k(t)}{2\pi} \quad (19)$$

B. Discrete-Time Energy Separation

Similarly, the discrete-time energy operator for the k-th mono-component signals in (1) must also be defined as [30]:

$$\Psi[\hat{s}_k(n)] = \hat{s}_k^2(n) - \hat{s}_k(n-1)\hat{s}_k(n+1) \quad (20)$$

where the derivatives $\dot{\hat{s}}_k$ are replaced by 2-samples backward (or forward) differences.

Thus, the discrete energy operator applied to $\hat{s}_k$ results in the following [30]

$$\Psi[\hat{s}_k(n)] = A_k^2\sin^2(\Omega_k) \quad (21)$$

where $\Omega_k = \omega_k T$ and T denotes the sampling period.

Likewise, the discrete energy operator for the first derivative of $\hat{s}_k(t)$ using a backward difference approximation becomes [30]

$$\Psi[r_k(n)] = 4A_k^2\sin^2(\Omega_k/2)\sin^2\Omega_k \quad (22)$$

where

$$r_k(n) = \hat{s}_k(n) - \hat{s}_k(n-1) \quad (23)$$

is the two-sample backward difference of $\hat{s}_k(t)$.

The expression in (22) may be combined with (21) and used to obtain the following expression

$$\frac{\Psi[r_k(n)]}{2\Psi[\hat{s}_k(n)]} = 2\sin^2(\Omega_k/2) = 1-\cos(\Omega_k) \quad (24)$$

Now, considering the above expressions, the DESA allows estimating instantaneous frequency and envelope which are expressed by [30]

$$\Omega_k(n) \approx \arccos\left(1-\frac{\Psi[r_k(n)]}{2\Psi[\hat{s}_k(n)]}\right) \quad (25)$$

$$A_k(n) \approx \sqrt{\frac{\Psi[\hat{s}_k(n)]}{1-\left(1-\frac{\Psi[r_k(n)]}{2\Psi[\hat{s}_k(n)]}\right)^2}} \quad (26)$$

C. Damping Estimate With Third-Order Energy Operators

In [36], new nonlinear operators differential in continuous-time and quadratic in discrete-time are presented to provide higher-order energy measurements. Accordingly, the third-order energy operator is adopted aiming to estimate the energy dissipation rate in damped oscillations in (1), since it represents a velocity operator that is suitable to track the changes in amplitude and phase with respect to the signal model in (1) and these changes are associated with damping and frequency. It is noteworthy to remark that the second and fourth order energy operators are related to position and acceleration, respectively. Thereby, the l^{th}-order discrete energy operator is defined by [36]:

$$\Psi_l[\hat{s}_k(n)] = \hat{s}_k(n)\hat{s}_k(n+l-2) - \hat{s}_k(n-1)\hat{s}_k(n+l-1) \quad (27)$$

Thus, for $l=3$ the third-order discrete energy operator results in

$$\Psi_3[\hat{s}_k(n)] = \hat{s}_k(n)\hat{s}_k(n+1) - \hat{s}_k(n-1)\hat{s}_k(n+2), \quad (28)$$

and $l=2$ corresponds to the discrete-time energy operator in (20), $\Psi_2[\hat{s}_k(n)] = \Psi[\hat{s}_k(n)]$.

The mono-component signals' discrete energy equations in the form of (1) are denoted by [36]

$$\Psi_l[\hat{s}_k(n)] = A_k^2 e^{2\sigma_k n+l-2}\sin\Omega_k\sin[(l-1)\Omega_k] \quad (29)$$

So, for $l=2$ and $l=3$, this becomes

$$\Psi_2[\hat{s}_k(n)] = A_k^2 e^{2\sigma n}\sin^2\Omega$$
$$\Psi_3[\hat{s}_k(n)] = A_k^2 e^{2\sigma_k+1}\sin\Omega_k\sin(2\Omega_k) \quad (30)$$

Notice that

$$\frac{\Psi_3[\hat{s}_k(n)]}{2\Psi_2[\hat{s}_k(n)]} = e^{\sigma_k}\cos\Omega_k \quad (31)$$

Meanwhile the damping may be estimated as

$$\hat{\sigma}_k(n) = \log\left(\frac{\Psi_3[\hat{s}_k(n)]}{2\Psi[\hat{s}_k(n)] - \Psi[r_k(n)]}\right) \quad (32)$$

Summarizing both frequency and damping ratio estimates can be computed as

$$\hat{f}_k(n) = \frac{\Omega_k(n)}{2\pi T_s} \quad (33)$$

and

$$\hat{\zeta}_k(n) = \frac{\sigma_k(n)}{\Omega_k(n)}, \quad (34)$$

respectively, where T_s is the sampling period.

Finally, the signal decomposition into mono-component signals is tackled by the IEVDHM technique aiming to estimate electromechanical modes from oscillatory signals. On the other hand, the instantaneous modal parameters' extraction is drawn by the DESA using (33)–(34).

Thus, the complete process to extract the modal features via IEVDHM-DESA is depicted by the flowchart in Fig. 1. To extract the mono-component signals contained in multiple signals stemming from PMUs, firstly, these signals are assembled into

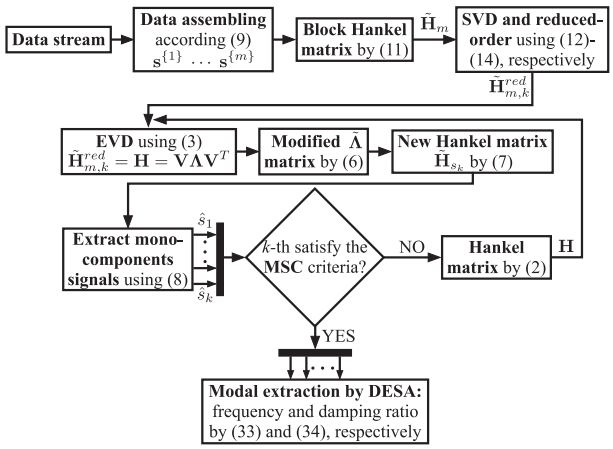

Fig. 1. Flowchart for applying the multivariate IEVDHM-DESA method to multiple output channels.

a matrix form according to (9). Afterwards, a block Hankel matrix using submatrices Hankel with the samples of each signal in (9) is constructed, as can be seen into (10)–(11). Now, to apply the EVD method for the first iteration, a reduced-order Hankel matrix is obtained by applying the SVD technique to the block Hankel matrix. This allows us to obtain a square Hankel matrix. Later, (6)–(8) are used to extract the mono-component signals. For the next iterations, the new Hankel matrices (one for each mono-component) are shaped using the samples of each mono-components extracted by (8) and constructed using (2), all this process is carried out in the iterative process until the *MSC* criterion is fulfilled for each extracted component. Once all mono-components are extracted, instantaneous modal parameters for each mono-component signal are estimated via the DESA using (33) and (34) for frequency and damping estimates, respectively.

IV. Performance of the IEVDHM-DESA Strategy for Electromechanical Modes Identification

To assess the performance of the multivariate IEVDHM-DESA strategy for modal identification; synthetic, simulated and real signals have been used to confirm the effectiveness of the proposal. These three test cases consist of: (*i*) multiple synthetic signals with three different modes and different damping levels; (*ii*) the New England power system; and (*iii*) a real power system event in the National Interconnected System (NIS) of Mexico. They are described in the following and compared with the Prony method and the well-known HHT due to its performance to decomposes non-linear and non-stationary signals [22].

A. Application to Multiple Synthetic Signals (Multivariate Analysis)

To demonstrate the multivariate performance of the proposed method and considering conditions for different damping ratio levels, where both damping ratio and frequency are exactly known, let's use multiple oscillating signals composed of the sum of the combined amplitude modulated (AM) primitive

TABLE I
Parameters for Multiple Synthetic Mixed Signals (Multivariate Analysis)

A_1	σ_1	f_1	A_2	σ_2	f_2	A_3	σ_3	f_3
12	0.0817	0.26	25	0.0081	0.43	20	0.4021	0.64
A_4	σ_4	f_4	A_5	σ_5	f_5	A_6	σ_6	f_6
12.01	0.0814	0.259	24.99	0.0081	0.431	20.01	0.4015	0.639
A_7	σ_7	f_7	A_8	σ_8	f_8	A_9	σ_9	f_9
11.99	0.0820	0.261	25.01	0.0081	0.429	19.99	0.4078	0.649

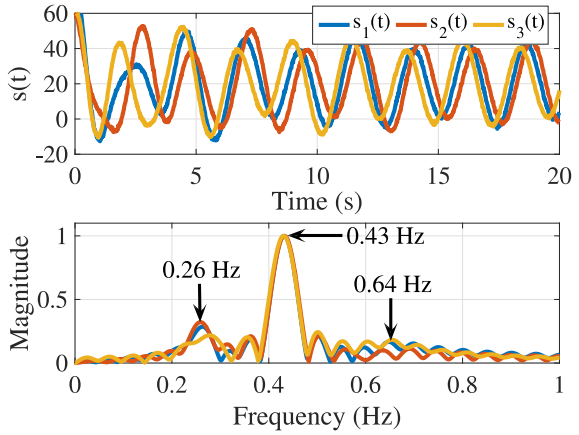

Fig. 2. Multiple synthetic signals (top plot) and their Fourier spectra (bottom plot).

signals, as follows:

$$s_1(t) = \sum_{k=1}^{3} A_k e^{\sigma_k t} cos(2\pi f_k t + \phi_k)$$

$$s_2(t) = \sum_{k=4}^{6} A_k e^{\sigma_k t} cos(2\pi f_k t + \phi_k)$$

$$s_3(t) = \sum_{k=7}^{9} A_k e^{\sigma_k t} cos(2\pi f_k t + \phi_k) \quad (35)$$

All parameters for signals s_1, s_2 and s_3 are summarized in Table I.

All multiple synthetic signals according to (35) and Table I are depicted in Fig. 2, where a DC component of 20 is also included. They contain the modal information indicated in Table I and their three modal frequencies can be seen in the Fourier spectra of the bottom plot of Fig. 2. Moreover, they are also polluted with white Gaussian noise (WGN) to achieve 15 dB of signal-to-noise ratio (SNR), and they use 60 Hz of sampling rate. Damping values in Table I represent medium, poor, and well-damped level modes, respectively.

By applying the proposed IEVDHM-DESA strategy in Fig. 1, mono-component signals are extracted from multiple oscillating signals through the multivariate IEVDHM method. To this end, all signals are assembled as in (9) and they are also used to construct a block Hankel matrix using (11), where a reduced-order matrix is obtained by means of SVD. Then, mono-component signals are extracted in an iterative way by employing (3), where for the first iteration the square reduced-order matrix Hankel is used, subsequently (6)–(8) are used. The next Hankel matrices

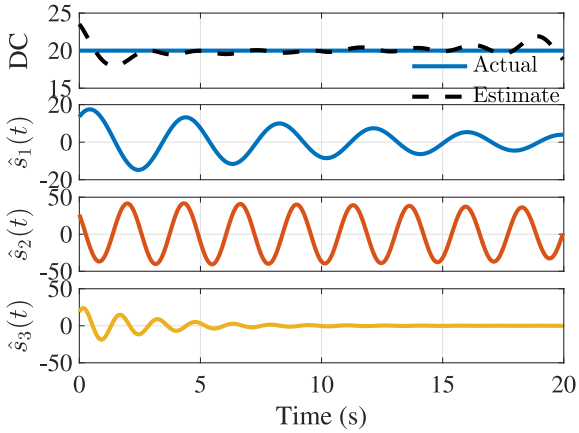

Fig. 3. Estimations of exponentially damped mono-components via the multivariate IEVDHM approach.

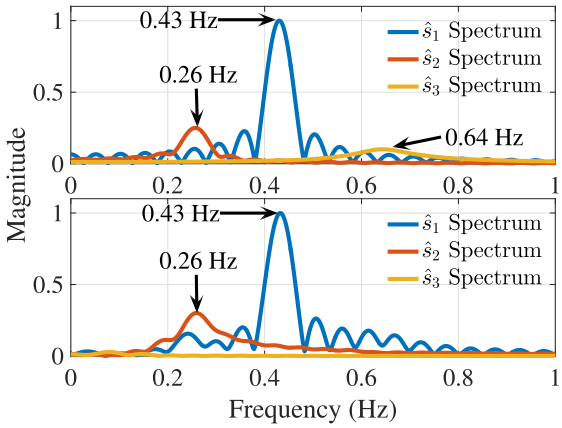

Fig. 4. Fourier spectra for exponentially damped mono-components: top plot using multivariate IEVDHM method and bottom plot using EMD method.

in the iterative process are formed using the mono-components extracted by (8) and using (2). Notice that this process is stopped when the *MSC* criterion is fulfilled for each extracted component as shown in Fig. 3. In a second stage, instantaneous modal parameters for each mono-component signal are also identified via the DESA, making use of (33) and (34) for achieving the frequency and damping estimations, respectively.

Notice that all multiple synthetic signals in the top plot of Fig. 2 are decomposed just into four components after conducting the multivariate analysis by the IEVDHM technique. So, Fig. 3 exhibits a DC component in the top plot, which is followed by modes with frequency components at 0.26, 0.43, and 0.64 Hz in the subsequent plots.

After evaluating the decomposition in time domain, the Fourier spectrum can also confirm the performance of the proposal in frequency domain. This is done by taking the Fourier's spectrum over mono-components captured by the multivariate IEVDHM approach, resulting in the top plot of Fig. 4, where the spectra for all mono-components are practically the same for the spectra of all synthetic signals in the bottom plot of Fig. 2. As can be observed, all three frequency spectra associated with the mono-components identified match with those frequency

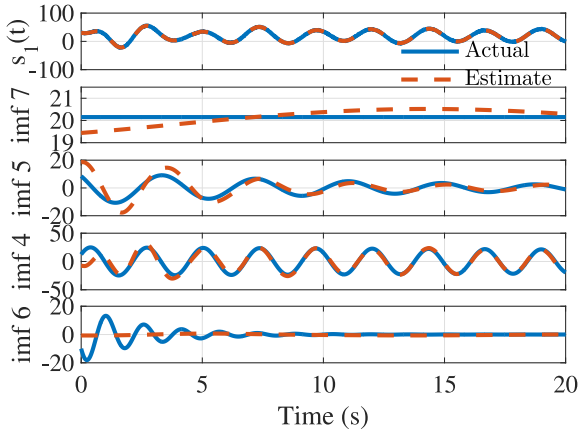

Fig. 5. Estimation of synthetic signal and IMFs representing mono-components through the EMD technique.

TABLE II
COMPARISONS BETWEEN THE IEVDHM-DESA, HHT, AND PRONY TECHNIQUES APPLIED TO A SYNTHETIC OSCILLATORY SIGNAL

Actual modes		**IEVDHM-DESA**		**HHT**		**Prony**	
Freq. (Hz)	Damp. ratio (%)	Freq. (Hz)	Damp. ratio (%)	Freq. (Hz)	Damp. ratio (%)	Freq. (Hz)	Damp. ratio (%)
0.2600	5.0000	0.2589	4.4198	0.2564	0.3665	0.2599	5.0401
0.4300	0.3000	0.4339	0.3983	0.4366	9.0786	0.4300	0.3002
0.6400	10.0000	0.6445	8.6304	—	—	0.6406	9.9997
–	–	–	–	–	–	0.9793	2.6482

components contained in the synthetic signals in (35). For that, the Fourier spectra are performed by removing the mean. It is noteworthy to remark that the multivariate IEVDHM method does not require detrending.

For comparison purposes, now the univariate EMD technique in [22] estimates the IMFs for the first signal in (35), resulting in seven mono-component signals, as displays in Fig. 5, where the IMFs 4-5 represent the dominant oscillatory components of the first synthetic signal in (35), whereas IMFs 1-3 and 6 are spurious modes, and IMF 7 contains the residue of the EMD algorithm which matches with the DC-component. In frequency domain, the bottom plot of Fig. 4 depicts the Fourier spectrum for IMFs 4-6 where it is noticed that the frequency of 0.64 Hz is missing. In this regard, the well-known Prony analysis is also applied to the first signal of (35) for comparing with our proposal, which it is implemented by means of a high-order Prony model fit (100th), then a lower order model is extracted retaining the dominant pairs of poles between 0.1 and 1 Hz [40]. This analysis results in four dominant modes in Table II, where the presence of a spurious mode is evident in the last row due to the added WGN to the synthetic signals.

Then, modal features are drawn by the DESA which depends on the discrete energy operators [30], [36]. Thus, instantaneous estimates of frequency $f_k(t)$ and damping ratio $\zeta_k(t)$ for the swing modes are illustrated in the top plots of Figs. 6 and 7, respectively. In contrast, the Hilbert transform [27] enables to gain instantaneous parameters that are depicted in the bottom plots of Figs. 6 and 7. Notice that the DESA outperforms the HHT estimates in both damping and frequencies. This fact is quantitatively summarized in Table II, where the comparison

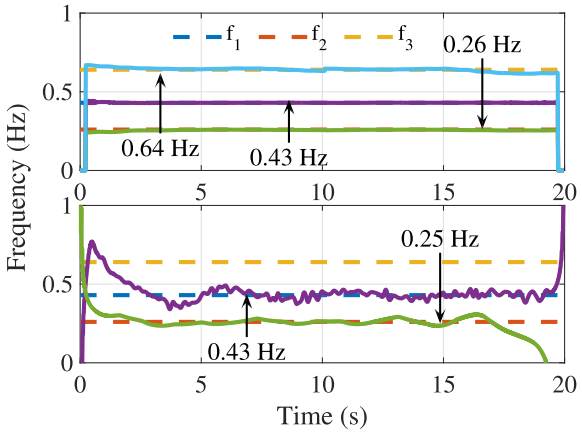

Fig. 6. Instantaneous frequency: top plot using the multivariate IEVDHM-DESA strategy and bottom plot using the HHT method.

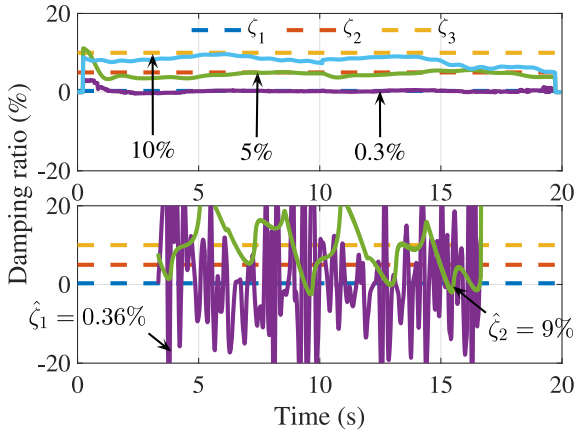

Fig. 7. Instantaneous damping ratio: top plot using multivariate IEVDHM-DESA method and bottom plot using HHT method.

between the multivariate IEVDHM-DESA estimate and the actual values of the synthetic signals in (35) are shown. The instantaneous parameters for both the multivariate IEVDHM-DESA and HHT methods are obtained by taking their average value. It is noticeable the presence of slight deviations in the damping estimations for the proposed technique, since the signal model approximation is intrinsically affected by the energy of the modes; likewise it is noteworthy that different damping levels in the electromechanical modes affect each other.

Since all modal information is available thanks to the time-frequency representation achieved by the multivariate IEVDHM and the extraction of dynamic patterns performed by the DESA, the multivariate IEVDHM-DESA's instantaneous frequency spectrum for all three modes contained in the synthetic mixed signals can be illustrated in Fig. 8. The vertical color bar indicates the normalized instantaneous energy at each point in the reconstructed mode ($\hat{s}_k$) which is derived as $E_k(t) = 1/2 * (\Omega_k^2 \times A_k^2)$. The first mode ($\hat{s}_1$) captures the effect at 0.26 Hz representing a medium-damped level mode of 5% ($\sigma_1 = 0.0817$), showing that its energy progressively decrease as the oscillation diminishes. The poor-damped level mode ($\hat{s}_2$) reveals its frequency component at 0.43 Hz with a σ_2 value of

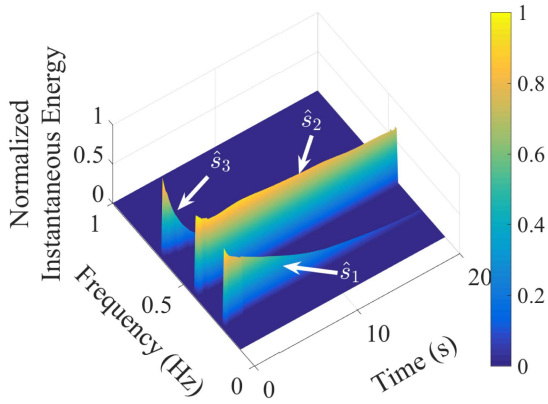

Fig. 8. Time-frequency representation for the modes contained into the synthetic mixed signals by using the multivariate IEVDHM-DESA spectrum.

TABLE III
ABSOLUTE ERROR FOR THE IEVDHM-DESA, HHT, AND PRONY METHODS IN CONTRAST TO THE ACTUAL DAMPING AND FREQUENCY VALUES

Absolute error					
IEVDHM-DESA		HHT		Prony	
Freq. (Hz)	Damp. ratio (%)	Freq. (Hz)	Damp. ratio (%)	Freq. (Hz)	Damp. ratio (%)
0.0011	0.5802	0.0036	4.6335	0.0001	0.0401
0.0039	0.0983	0.0066	8.7786	0.0000	0.0002
0.0045	1.3696	—	—	0.0006	0.0003
—	—	—	—	0.9793	2.6482

0.0081, exhibiting significant changes in the energy after 10 s. The IEVDHM-DESA spectrum of the third mode ($\hat{s}_3$) displays the well-damped level of 10% ($\sigma_3 = 0.4021$), it also exhibits the complete attenuation of the mode before 10 s, which can be correlated with the third plot in Fig. 3.

Finally, the absolute error of each method in Table III is taken employing the actual values as reference to exhibit the performance of the method in the condition with changing damping ratio, where damping ratio is exactly known. Despite the high accuracy of the Prony analysis for the first three dominant modes, this also provides a fourth mode in the selected frequency range due to the added WGN.

B. Application to the New England Power Grid

In this section, the IEVDHM-DESA strategy for multiple channels is applied to simulated signals obtained from the well-known 16-machine test power system, which contains 68-bus in [41]. Emphasis is made on the electromechanical modes with lower frequency, conventionally associated with inter-area oscillations. To this end, transient stability simulations are carried out using *s_simu* function in the power system toolbox (PST). In this simulation, a 3-cycle three-phase short-circuit is applied to bus 16 (Medway substation) exciting the system dynamics, which is cleared tripping the interconnection line with bus 15 (Sherman Rd. substation).

According to the location of the measurements, three analysis scenarios are derived from simulation, thereby measurements are taken at: (*S1*) all generator rotor angle speeds are considered; (*S2*) all angular differences among voltage angles of the nearest bus to every generator, as results of the participation factors

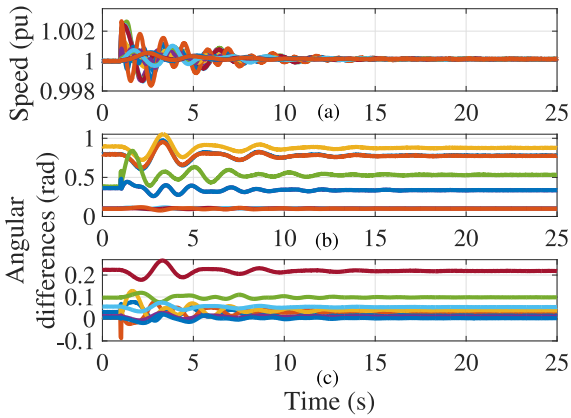

Fig. 9. Three analysis scenarios for the New England grid. (a) Scenario *S1*, (b) scenario *S2*, and (c) scenario *S3*.

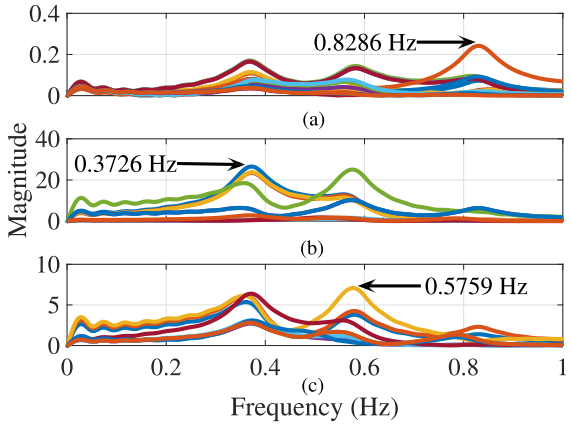

Fig. 10. Fourier's spectra for the three scenarios. (a) Scenario *S1*, (b) scenario *S2*, and (c) scenario *S3*.

(only those associated with the rotor angle speed) that are greater than 0.2 in the small-signal analysis (SSA); and (*S3*) all angular differences among voltage angles of the buses at each tie-line among areas.

In all three scenarios, signals are also contaminated with WGN, achieving an SNR of 15 dB, as can be seen in Fig. 9. Afterwards, Fourier spectra are taken, resulting in three inter-area modes for all scenarios at 0.3726, 0.5759, and 0.8286 Hz, which can be identified in Fig. 10.

The application of the multi-dimensional IEVDHM algorithm described in Section II-B is carried out over the aforementioned scenarios, gaining an optimal set of mono-component signals that closely represent the underlying electromechanical dynamics of the system. To quantitatively contrast the proposal against the HHT (only for generator G1), VMD, and multi-Prony techniques, the scenario *S1* is analyzed resulting in the modes summarized in Table IV, when the inputs of the methods are generator's rotor angle speeds. For this scenario, all techniques behave in accordance to the frequencies in the Fourier spectra.

For the sake of brevity, scenario *S2* is only exhibited in Figs. 11, 12. Where the plots (a)-(c) of Fig. 11 show the extraction in time of three dominant oscillatory modes at 0.3776, 0.5793, and 0.8263 Hz, which match with those captured by the

TABLE IV
MULTI-DIMENSIONAL IEVDHM-DESA COMPARED AGAINST THE HHT, VMD AND MULTI-PRONY METHODS IN SCENARIO *S1*

Generator's rotor angle speeds for *S1*							
IEVDHM-DESA		**HHT for G1**		**VMD** [27]		**Multi-Prony**	
Freq. (Hz)	Damp. ratio (%)	Freq. (Hz)	Damp. ratio (%)	Freq. (Hz)	Damp. ratio (%)	Freq. (Hz)	Damp. ratio (%)
0.3671	11.3596	0.3672	11.8111	0.3647	11.7258	0.3665	10.9141
0.5795	5.6537	0.5711	8.0504	0.5654	6.6725	0.5728	7.0017
0.8249	4.5477	—	—	0.8226	5.4012	0.8260	4.9404

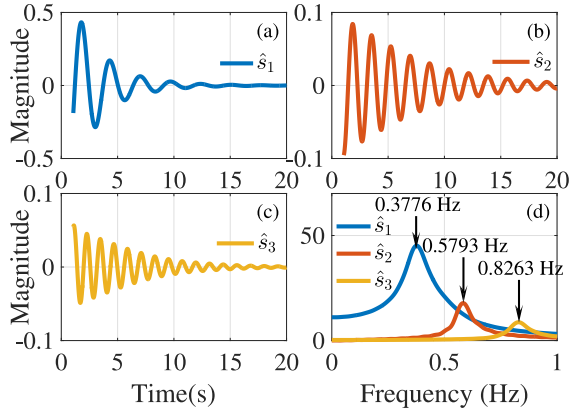

Fig. 11. Optimal set of modes in scenario *S2*. (a) Mode at 0.3776 Hz. (b) Mode at 0.5793 Hz. (c) Mode at 0.8263 Hz. (d) Fourier's spectra for each mode.

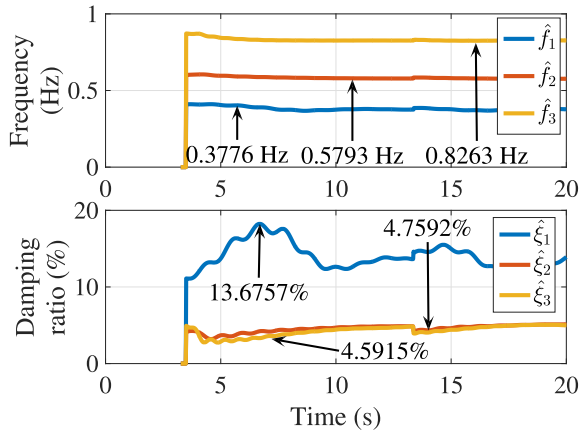

Fig. 12. Instantaneous modal estimates provided by the IEVDHM-DESA strategy (top plot the frequency and bottom plot the damping ratio) for the interarea modes in scenario *S2*.

Fourier spectra in Fig. 10. To corroborate the correct decomposition in frequency, Fourier's spectra for the optimal set of mono-component signals are displayed in the plot (d) of Fig. 11, demonstrating that the signal decomposition in frequency domain is quite precise since the modal information also matches with that in Fig. 10.

Fig. 12 depicts the instantaneous global frequency (top plot) and damping ratio (bottom plot) in scenario *S2*, this modal information is extracted from the analyzed signals using the DESA by applying (33) and (34), respectively. Smooth frequency estimates are displayed. Slight deviations in damping estimations are affected by the presence of different damping levels and the energy of the modes.

TABLE V
COMPARISON BETWEEN MULTI-DIMENSIONAL IEVDHM-DESA AND MULTI-PRONY METHODS IN SCENARIOS *S2* AND *S3*

Scenario *S2* (Participation factors)				Scenario *S3* (Tie-lines)			
IEVDHM-DESA		**Multi-Prony**		**IEVDHM-DESA**		**Multi-Prony**	
Freq. (Hz)	Damp. ratio (%)	Freq. (Hz)	Damp. ratio (%)	Freq. (Hz)	Damp. ratio (%)	Freq. (Hz)	Damp. ratio (%)
0.3776	13.6757	0.3695	11.7402	0.3723	12.4463	0.3690	11.6037
0.5793	4.7592	0.5734	6.9990	0.5743	4.5088	0.5719	6.5977
0.8263	4.5915	0.8209	4.7665	0.8198	4.1895	0.8139	4.7738
–	–	0.2141	183.3258	–	–	0.4427	68.1463

Comparisons between the proposed method and the multi-Prony analysis are established in Table V, when input signals are based on scenarios *S2* and *S3*. The Prony analysis has been implemented for processing multiple channels. It is noteworthy that the IEVDHM-DESA strategy precisely captures all three dominant modes in the New England power grid. Regarding the Prony approach, spurious modes are identified at 0.2141 and 0.4427 Hz in scenarios *S2* and *S3*, due to the added WGN to the simulated signals.

C. Application to a Real System Event in the NIS of Mexico

In Mexico there are four electrical systems that operate in isolation, Muleje, Baja California (BCA), Baja California Sur (BCS), and the NIS which is the largest one. The total installed capacity is approximately 83,120MW with a maximum demand about 50GW in 2019. The BCA system is interconnected to the California ISO (CAISO) through two synchronous 230 kV transmission lines (TL).

The NIS is a mesh system with radial connections towards the northwest and southeast. Its transmission level is mainly composed of TLs with operating voltages of 400 kV, 230 kV and 130-69 kV. This system covers from Quintana Roo to Sonora state, making up the main electrical power grid in Mexico, and it is split into 7 regions: Central, Eastern, Western, Northwestern, North, Northeastern, and Peninsular. It also has six trade international interconnections: (*i*) there are four asynchronous connections in the Northeastern region with the Electric Reliability Council of Texas (ERCOT) in USA by four tie-lines with 436MW capacity; (*ii*) there is one synchronous connection in the Eastern region with Guatemala via one tie-line with 240MW capacity; and (*iii*) there is also one synchronous connection in the Peninsular region with Belize by one tie-line with 55MW capacity. For the sake of brevity, public official documents are available at [42].

On Dec 28^{th}, 2020 two of the main TLs that interconnect the Northwestern, North and Northeastern regions with the Central, Eastern, Western and Peninsular regions were tripped provoking a cascade event that tripped other TLs, such as the interconnection with Guatemala. Due to the loading capacity of TLs and the presence of power oscillations, the Northwestern, North and Northeastern regions remained connected with the Central, Eastern, Western and Peninsular by one TL. Thus, this sequence of events yielded that the power generation surpassed the load demand in the Northwestern, North and Northeastern, causing a frequency excursion up to 61.14 Hz that activated the stages of remedial action schemes to trip generation derived from high frequency. Meanwhile the load demand surpassed

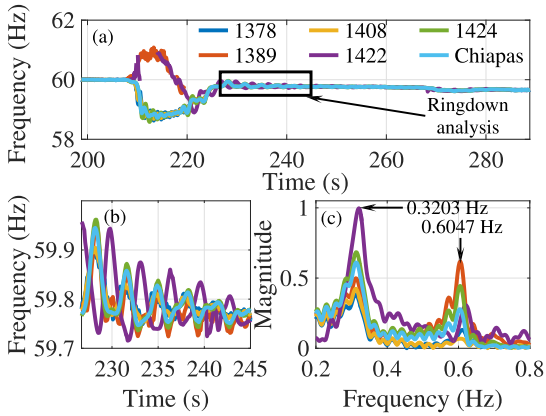

Fig. 13. Frequency measurements captured by 5 FDRs and 1 PMU in the NIS. (a) Real event measurements. (b) Ringdown analysis and (c) their Fourier's spectra.

the power generation in the Central, Eastern, Western, and Peninsular regions, dropping down the frequency up to 58.76 Hz and activating the load shedding stages as a consequence of the low frequency. As a result, the total affectation of power generation and load reached 8,696MW, representing 26% of the demand [42].

This case comprises the recorded measurements in the mentioned event, which are collected by five time-synchronize frequency disturbance recorders (FDRs) and a PMU installed in the following locations: 1389-Monterrey (Northeastern), 1422-Mazatlan (Northwestern), 1378-Guadalajara and 1408-Morelia (both Western), and 1424-Chetumal (Peninsular), and PMU-Chiapas (Eastern). Numbers denote the ID code for FDRs in the FNET/GridEye project.[1] The collected measurements from five regions are illustrated in Fig. 13(a), where the measurements 1389, 1422 exhibited a frequency increment, whereas the measurements 1378, 1408, 1424, and Chiapas presented a frequency drop. For this real event, the length of the window analysis is adopted of 20 s, as shown in Fig. 13(b). Likewise, their Fourier's spectra are displayed in Fig. 13(c), where two oscillating modes are indicated at 0.32 and 0.60 Hz.

Once the measurements are available, the multi-dimensional IEVDHM-based time-frequency analysis is accomplished finding two dominant modes, as depicted in the plots (a)-(b) of Fig. 14, where it is noticeable decaying amplitudes and homogeneous frequencies in each mono-component in the time domain. In the frequency domain, Fourier's spectra of the optimal set of mono-component signals are illustrated in the plot (c) of Fig. 14, where the precise TFR of multi-component non-stationary signals attained can be observed, where two inter-area modes are separated into mono-component signals.

The extraction of instantaneous modal parameters achieved by the DESA results in two dominant modes, as illustrated in Fig. 15, where instantaneous modal frequencies and instantaneous damping ratios are shown in the top and bottom plots, respectively. Notice that both precisely match with those captured by the FFT in Fig. 13(c).

[1][Online]. Available: http://fnetpublic.utk.edu/index.html

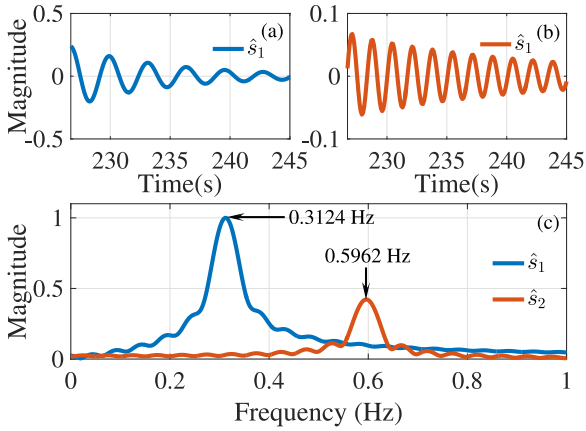

Fig. 14. Optimal set of modes for a NIS real oscillatory event. (a) Mode at 0.3124 Hz. (b) Mode at 0.5962 Hz. (c) Fourier's spectra for each mode.

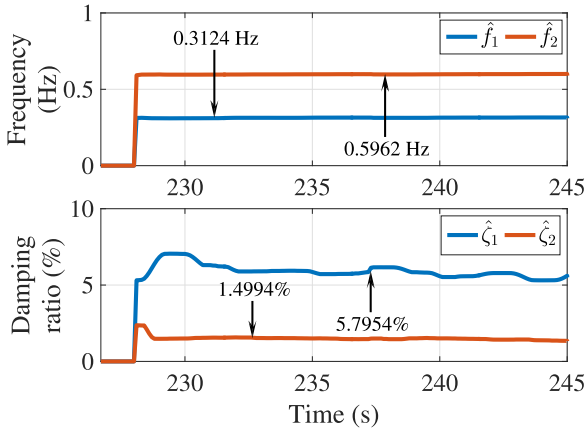

Fig. 15. Instantaneous modal estimates provided by the IEVDHM-DESA strategy (top plot the frequency and bottom plot the damping ratio) for modes at 0.3124 Hz and 0.5962 Hz in the Mexican Interconnection.

TABLE VI
COMPARISON BETWEEN THE MULTI-DIMENSIONAL IEVDHM-DESA AND HHT METHODS APPLIED TO THE NIS POWER GRID

FFT	IEVDHM-DESA		HHT for unit 1424		Multi-Prony	
Freq. (Hz)	Freq. (Hz)	Damp. ratio (%)	Freq. (Hz)	Damp. ratio (%)	Freq. (Hz)	Damp. ratio (%)
0.3203	0.3124	5.7954	0.3276	2.4787	0.3168	5.6331
0.6047	0.5962	1.4994	—	—	0.6114	1.2935
–	–	–	–	–	0.2295	31.4468
–	–	–	–	–	0.4227	10.0003
–	–	–	–	–	0.6026	9.6882
–	–	–	–	–	0.7395	6.0103
–	–	–	–	–	0.8405	4.6656
–	–	–	–	–	0.9485	4.5371

For comparison purposes, the real oscillating signal stemming from the unit 1424 is also decomposed by the EMD technique, then its IMFs are extracted and their instantaneous modal parameters are estimated by the HT. Table VI summarizes the average values of instantaneous frequencies and damping ratios for both the multi-dimensional IEVDHM-DESA and HHT techniques. When the multi-Prony analysis is performed, two modes are correctly identified as depicts in Table VI, however the existence of other 6 spurious modes with different damping

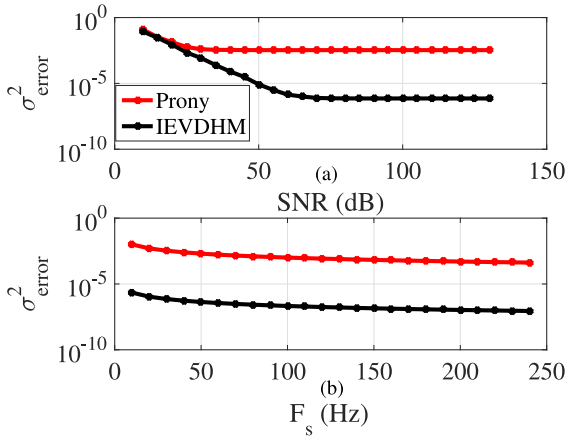

Fig. 16. Sensitivity analysis for different: (a) noise levels and (b) sampling rates.

levels is evident and the second and fifth modes have similar frequencies in comparison with the second frequency in the Fourier spectrum.

D. Sensitivity Analysis

To validate the good performance of the proposed methodology, sensitivity analyses are conducted for different noise levels and sampling rates and compared with the Prony method. These analyses are carried out over the synthetic mixed signals in (35).

The noise tolerance analysis is performed quantifying the impact of SNR variations on the output variance as describes in [27], resulting in Fig. 16(a), where the IEVDHM presents low sensitivity to noise, reaching the minimum output variance at 7.97×10^{-07} in 70 dB. Meanwhile for Prony method, the output variance decreases as SNR increases, and becomes higher than that of the IEVDHM. Similarly, the sampling rate analysis is conducted by evaluating the impact of the output variance to sampling frequency variations. The attained results in Fig. 16(b) show that the IEVDHM keeps decreasing up from 2.2×10^{-06} for $F_s = 10$ Hz until reaching the minimum output variance at 8.84×10^{-08} for $F_s = 240$ Hz. It is noteworthy that the proposed method has a low sensitivity for different SNR conditions and sampling rates, since it exhibits a suitable performance at $F_s = 10$ Hz which corresponds to the minimum sampling frequency in this investigation.

The sensitivity analyses have demonstrated that the proposed method in comparison with the Prony method is capable to eliminate the spurious modes by means of its iterative process. The IEVDHM method has a low sensitivity to noise (see Fig. 16(a)), where the search of polynomial roots is not needed as in Prony analysis [40], besides the proposal obtains instantaneous values of frequency and damping for non-stationary signals thanks to the DESA. The complexity of the method can be reduced using low sampling rates (see Fig. 16(b)).

E. Computational Analysis

Considering all the required computations in Section II, it is noteworthy that the most demanding tasks are associated with

TABLE VII
SIZE OF THE HANKEL MATRIX

	Synthetic	New England	Real event in Mexico
Sampling freq.	60 Hz	60 Hz	10 Hz
$\mathbf{H} \in \Re^{N \times N}$	600×600	600×600	100×100

TABLE VIII
OVERALL EXECUTION TIME PER WINDOW AND NUMBER OF ITERATIONS PER MODE FOR SYNTHETIC, NEW ENGLAND, AND REAL EVENT CASES

	Synthetic	New England	Real event in Mexico
No. of signals	1	16	6
Window length	7.69s	5.45s	20s
IEVDHM-DESA	1.3329s	3.1222s	0.1367s
Multi-Prony	0.6153s	12.78s	0.1459s
No. iterations per mode	Mode 1: 0 Mode 2: 3 Mode 3: 2	Mode 1: 0 Mode 2: 2 Mode 3: 2	Mode 1: 2 Mode 2: 1 —

the SVD and the iterative eigenvalue decomposition. The execution of all these tasks impacts the estimation time per analysis window, making the proposed method suitable for post-mortem analysis. This fact is associated with the size of the Hankel matrix since it is directly related to the parameter N and in turn, this is directly related to the sampling frequency; then, the size of the Hankel matrix in (14) varies accordingly. This is shown in Table VII, where the size of the Hankel matrix increases by 10 times the sampling frequency for each case. Nevertheless, the average execution time over 10 times and the number of iterations per mode for synthetic, New England (S1) and real event signals are summarized in Table VIII; likewise the number of iterations per mode that the IEVDHM performs to converge, is presented in Table VIII. It is remarkable that despite the number of iterations implied during the iterative eigendecomposition, the execution time of the IEVDHM-DESA method is at least four times faster than that of the multi-Prony analysis when 16 channels are analyzed simultaneously. All these computations are achieved using a Python-based environment embedded in a desktop running Windows 10 with Intel(R) Xeon(R) CPU E5-1620 v4, 3.5 GHz, 32 GB RAM, and 64-bit. The code for the algorithms is online available in [42].

V. CONCLUSION

This paper has successfully demonstrated that a new strategy based on a time-frequency representation and an energy operator can decompose single or multiple non-stationary multi-component signals into mono-component signals and provide modal patterns associated with electromechanical oscillations. The principal idea behind this strategy consists of an iterative eigenvalue decomposition of the square Hankel matrix constructed from samples of a set of multi-component non-stationary signals, which is strengthened by an instantaneous stage for the modal information extraction. The iterative process of the Hankel matrix ends when all extracted eigenvalues fulfill the mono-component signal criteria. After all modes are identified, they are processed by the discrete-time energy operator to provide instantaneous modal parameters, such as frequency and damping. The proposed strategy was tested by using simulated and real signals. Despite high noisy conditions were involved to corroborate its noise tolerance, the method reached accurate approximations in capturing modal information. Thus, the proposed approach supported by the IEVDHM and the DESA makes up a powerful tool for extraction of modal information in power systems, given by its reliable results.

Since the proposed method is intended to work for post-mortem analysis, then it can be used to: increase the low identification performance of power oscillation events due to its capability of differentiating concurrent modes with close frequencies, support the off-line contingency analysis, support the post-disturbance scenario reconstruction, and tune controllers that mitigate power oscillations. Its main drawback is derived from its computational complexity and the considerable window length which prevent its use from an on-line application.

ACKNOWLEDGMENT

The authors would like to thank to the Power Information Technology Lab and the FNET/GridEye project lead by Prof. Yilu Lu for the real network data provided.

REFERENCES

[1] Z. Tashman, H. Khalilinia, and V. Venkatasubramanian, "Multi-dimensional fourier ringdown analysis for power systems using synchrophasors," *IEEE Trans. Power Syst.*, vol. 29, no. 2, pp. 731–741, Mar. 2014.
[2] University of Tennessee at Knoxville, "Fnet/grideye frequency display," May 2018. [Online]. Available: http://fnetpublic.utk.edu/tabledisplay.html
[3] Indian Institute of Technology, "Wide area frequency measurement system," May 2018. [Online]. Available: http://103.7.128.82/rwafms/wafms/
[4] A. Zamora, V. M. Venkatasubramanian, J. A. de laO. Serna, J. M. Ramirez, and M. Paternina, "Multi-dimensional ringdown modal analysis by filtering," *Electric Power Syst. Res.*, vol. 143, pp. 748–759, 2017.
[5] J. Y. Cai, Z. Huang, J. Hauer, and K. Martin, "Current status and experience of wams implementation in north america," in *Proc. IEEE/PES Transmiss. Distrib. Conf. Exposition: Asia Pacific*, 2005, pp. 1–7.
[6] J. Sanchez-Gasca and D. Trudnowski, "Identification of electromechanical modes in power system," *IEEE PES Task Force Identification Electromech. Modes Power Syst. Stability*, Piscataway, NJ, USA, Tech. Rep. Rep. PES-TR15, Jun. 2012.
[7] R. Cardenas-Javier *et al.*, "A matlab and powerfactory-based wams simulator," in *Proc. North Amer. Power Symp.*, 2019, pp. 1–6.
[8] M. G. Frei and I. Osorio, "Intrinsic time-scale decomposition: Time-frequency-energy analysis and real-time filtering of non-stationary signals," *Proc. Roy. Soc. A-Math. Phys.*, vol. 463, no. 2078, pp. 321–342, 2007.
[9] P. Jain and R. B. Pachori, "An iterative approach for decomposition of multi-component non-stationary signals based on eigenvalue decomposition of the hankel matrix," *J. Franklin Inst.*, vol. 352, no. 10, pp. 4017–4044, 2015.
[10] B. Boashash, *Time-Frequency Signal Analysis and Processing: A Comprehensive Reference*. Cambridge, MA, USA: Academic Press, 2015.
[11] Y. Jiang and Y. He, "Frequency estimation of electric signals based on the adaptive short-time fourier transform," *Int. J. Electron.*, vol. 96, no. 3, pp. 267–279, 2009.
[12] R. R. Sharma and R. B. Pachori, "Improved eigenvalue decomposition-based approach for reducing cross-terms in Wigner-Ville distribution," *Circuits, Systems, Signal Process.*, vol. 37, no. 8, pp. 3330–3350, 2018.
[13] I. Daubechies, *Ten Lectures on Wavelets*. Philadelphia, PA, USA: SIAM, 1992.
[14] H. Ahmed and A. K. Nandi, *Condition Monitoring With Vibration Signals*. Hoboken, NJ, USA: Wiley Online Library, 2019.

[15] Ç. P. Dautov and M. S. Özerdem, "Wavelet transform and signal denoising using wavelet method," in *Proc. 26th Signal Process. Commun. Appl. Conf.*, 2018, pp. 1–4.
[16] Y. Meyer, *Wavelets and Operators: Volume 1*. Cambridge, U.K.: Cambridge Univ. Press, 1992.
[17] C.-W. Kok and W.-S. Tam, *Digital Image Interpolation in Matlab*. Hoboken, NJ, USA: John Wiley & Sons, Inc., 2019.
[18] B. Boashash and P. Black, "An efficient real-time implementation of the wigner-ville distribution," *IEEE Trans. Acoust., Speech, Signal Process*, vol. 35, no. 11, pp. 1611–1618, Nov. 1987.
[19] N. A. Khan, I. A. Taj, M. N. Jaffri, and S. Ijaz, "Cross-term elimination in wigner distribution based on 2D signal processing techniques," *Signal Process.*, vol. 91, no. 3, pp. 590–599, 2011.
[20] R. B. Pachori and P. Sircar, "A new technique to reduce cross terms in the wigner distribution," *Digit. Signal Process.*, vol. 17, no. 2, pp. 466–474, 2007.
[21] N. Huang, "The empirical mode decomposition and hilbert spectrum for nonlinear and nonstationary time series analysis," *Proc. Roy. Soc. London A*, vol. 454, pp. 903–995, 1998.
[22] A. R. Messina and V. Vittal, "Nonlinear, non-stationary analysis of inter-area oscillations via hilbert spectral analysis," *IEEE Trans. Power Syst.*, vol. 21, no. 3, pp. 1234–1241, Aug. 2006.
[23] X. Hu, S. Peng, and W.-L. Hwang, "EMD revisited: A new understanding of the envelope and resolving the mode-mixing problem in AM-FM signals," *IEEE Trans. Signal Process.*, vol. 60, no. 3, pp. 1075–1086, Mar. 2012.
[24] Z. Wu and N. E. Huang, "Ensemble empirical mode decomposition: A noise-assisted data analysis method," *Ad. Adaptive Data Analy.*, vol. 1, no. 01, pp. 1–41, 2009.
[25] B. Yan, X. Cheng, and F. Chen, "Single-phase voltage sag detection algorithm based on ensemble empirical mode decomposition and two-points method," in *Proc. Chin. Autom. Congr.*, 2019, pp. 2500–2505.
[26] K. Dragomiretskiy and D. Zosso, "Variational mode decomposition," *IEEE Trans. Signal Process.*, vol. 62, no. 3, pp. 531–544, Feb. 2014.
[27] M. R. Arrieta Paternina, R. K. Tripathy, A. Zamora-Mendez, and D. Dotta, "Identification of electromechanical oscillatory modes based on variational mode decomposition," *Electric Power Syst. Res.*, vol. 167, pp. 71–85, 2019.
[28] J. Kaiser, "On a simple algorithm to calculate the 'energy' of a signal," in *Proc. Int. Conf. Acoust., Speech, Signal Process.*, 1990, pp. 381–384.
[29] J. F. Kaiser, "Some useful properties of teager's energy operators," in *Proc. IEEE Int. Conf. Acoust., Speech, Signal Process.*, 1993, pp. 149–152.
[30] P. Maragos, J. F. Kaiser, and T. F. Quatieri, "Energy separation in signal modulations with application to speech analysis," *IEEE Trans. Signal Process.*, vol. 41, no. 10, pp. 3024–3051, Oct. 1993.
[31] I. Kamwa, A. K. Pradhan, and G. Joós, "Robust detection and analysis of power system oscillations using the teager-kaiser energy operator," *IEEE Trans. Power Syst.*, vol. 26, no. 1, pp. 323–333, Feb. 2011.
[32] P. Jain and R. B. Pachori, "GCI identification from voiced speech using the eigen value decomposition of hankel matrix," in *Proc. 8th Int. Symp. Image Signal Process. Anal.*, 2013, pp. 371–376.
[33] R. R. Sharma and R. B. Pachori, "Time-frequency representation using IEVDHM-HT with application to classification of epileptic EEG signals," *IET Sci., Meas. Technol.*, vol. 12, no. 1, pp. 72–82, 2017.
[34] R. R. Sharma, M. Kumar, and R. B. Pachori, "Joint time-frequency domain-based CAD disease sensing system using ECG signals," *IEEE Sensors J.*, vol. 19, no. 10, pp. 3912–3920, May 2019.
[35] R. R. Sharma, M. Kumar, S. Maheshwari, and K. P. Ray, "EVDHM-ARIMA-based time series forecasting model and its application for COVID-19 cases," *IEEE Trans. Instrum. Meas.*, vol. 70, 2021, Art no. 6502210, doi: 10.1109/TIM.2020.3041833.
[36] P. Maragos and A. Potamianos, "Higher order differential energy operators," *IEEE Signal Process. Lett.*, vol. 2, no. 8, pp. 152–154, Aug. 1995.
[37] F. Salzenstein, A.-O. Boudraa, and J.-C. Cexus, "Generalized higher-order nonlinear energy operators," *JOSA A*, vol. 24, no. 12, pp. 3717–3727, 2007.
[38] J. Hauer, C. Demeure, and L. Scharf, "Initial results in prony analysis of power system response signals," *IEEE Trans. Power Syst.*, vol. 5, no. 1, pp. 80–89, Feb. 1990.
[39] H. M. Teager and S. M. Teager, "Evidence for nonlinear sound production mechanisms in the vocal tract," in *Speech Prod. Modelling*, vol. 55. D.W. J. Hardcastle and A. Marchal, Eds. Boston, MA, USA: Kluwer, Jul. 1989, pp. 17–29.
[40] P. W. Sauer *et al.*, *Power System Dynamics and Stability*. Hoboken, NJ, USA: John Wiley & Sons, Inc., 2016.
[41] J. A. de laO. Serna, J. M. Ramirez, A. Zamora Mendez, and M. R. A. Paternina, "Identification of electromechanical modes based on the digital taylor-fourier transform," *IEEE Trans. Power Syst.*, vol. 31, no. 1, pp. 206–215, Jan. 2016.
[42] R. Reyes, M. Paternina, A. Zamora, J. de la, and O. Serna, "Iterative mode decomposition", 2021, Accessed: May 9, 2021. [Online]. Available: https://github.com/rreyesdeluna/Iterative_Mode_Decomposition.git